PERGAMON

International Journal of Solids and Structures 40 (2003) 6527–6545

INTERNATIONAL JOURNAL OF SOLIDS and STRUCTURES

www.elsevier.com/locate/ijsolstr

Out-of-plane static analysis of circular arches by DQM

P. Malekzadeh [a], G. Karami [b,*]

[a] Department of Mechanical Engineering, Shiraz University, Shiraz 71345, Iran

[b] Department of Mechanical Engineering and Applied Mechanics, North Dakota State University, Fargo, ND 58105, USA

Received 1 July 2002; received in revised form 9 July 2003

Abstract

The differential quadrature (DQ) methodology introduced by the authors [see, Comput. Methods Appl. Mech. Engng. 191 (2002a) 3509; Int. J. Solids Struct. 39 (19) (2002b) 4927; Int. J. Numer. Methods Engng. 54 (3) (2003a) 847; J. Sound Vibrat. 263 (2) (2003b) 415] is employed for out-of-plane static analysis of circular arches under a wide spectrum of boundary conditions. In addition to the classical boundary conditions, elastic restraints against translation and rotation are also considered. Different loading conditions are examined. Several examples of arches with uniform, continuous or stepped varying cross-sections are presented to demonstrate the accuracy of the methodology. The domain decomposition technique in conjunction with the present DQ methodology is examined for certain cases. The results are compared with those of exact solutions for several uniform or stepped sections arches and also for arches on elastic foundations. Accurate converged numerical solutions are obtained with only few grid points.

Keywords: Circular arch; Out-of-plane static analysis; Elastic foundations; Differential quadrature method; Domain decomposition

1. Introduction

Finite element and finite difference methods have been widely used for the solution of circular arch structures. Employing low order approximation schemes in these methods may result in stress distributions of oscillatory nature. To obtain highly accurate solutions, fine meshing should be used. Sophisticated quantic–quantic or hybrid finite elements with high degrees of freedom may also be employed with excessive number of elements to obtain satisfactory solutions (Tong et al., 1998). The differential quadrature method (DQM) can be used as an efficient numerical algorithm in this respect to cover some drawbacks of other methods. DQM has been widely employed for the analysis of solid mechanics problems in recent years. The details on the development and its implementation can be found in review papers by Bert and Malik (1996, 1997). A major drawback in conventional DQ methods is the difficulty in boundary condition implementations for differential equations with multiple boundary conditions at the boundary points.

* Corresponding author.
E-mail address: G.Karami@ndsu.nodak.edu (G. Karami).

0020-7683/$ - see front matter © 2003 Elsevier Ltd. All rights reserved.
doi:10.1016/S0020-7683(03)00412-8

There has been a considerable effort to overcome this problem, especially for fourth-order governing differential equations of classical beam and plate problems. These efforts will include the introduction of the well known δ-technique (Bert and Malik, 1996), modified weighing coefficients (Wang and Bert, 1993; Malik and Bert, 1996), SBCGE and CBCGE coefficients of Shu and Du (1997a,b), and other methodologies that assume the first derivative on the boundary as additional degrees of freedom (Chen et al., 1997; Wang and Gu, 1997; Wang et al., 1998; Wu and Liu, 2000, 2001; De Rosa and Franciosi, 1998a,b, 2000). On this matter, an alternative methodology based on defining the second derivatives of the field variable only at the boundary points as independent degrees of freedom were introduced by the authors (Karami and Malekzadeh, 2002a,b, 2003a,b).

The static governing equations of the thin arches include fourth and second-order differential equations. Solution to such system of equations using the newly developed DQ methodology by the authors is a matter of interest in this paper. Circular arches with different cross-sectional geometries, i.e. uniform, continuously varying and stepped cross-section, under different loading conditions would be considered here. The generality of the methodology would be demonstrated by considering different types of classical and non-classical boundary conditions. Based on the proposed methodology, a domain decomposition technique for the cases with discontinuities in geometries, loadings or material properties is presented. As an application, the ring on elastic foundation with a series of point loads (Volterra, 1951), a rather important practical problem is to be analyzed. Examples on arches having discontinuities in geometrical and material properties and also on arches with non-uniform cross-sections are presented.

2. Governing equations

The governing equations for out-of-plane response of a variable section circular arch are derived based on the classical beam theory. The degrees of freedom are out-of-plane displacement v, and the angle of twist φ. The total potential energy of circular arches for out-of-plane response can be written as (Yoo and Fehrenbach, 1981),

$$\pi = \frac{1}{2}\int_0^{\theta_0}\left[\frac{EI_x}{R}\left(\frac{1}{R}\frac{\mathrm{d}^2 v}{\mathrm{d}\theta^2}-\varphi\right)^2+\frac{GJ}{R}\left(\frac{1}{R}\frac{\mathrm{d}v}{\mathrm{d}\theta}+\frac{\mathrm{d}\varphi}{\mathrm{d}\theta}\right)^2-p_y R v-t_z R\varphi\right]\mathrm{d}\theta+\frac{k_{1l}v_{(0)}^2}{2}+\frac{k_{2l}v_{(\theta_0)}^2}{2}$$
$$+\frac{k_{1t}\varphi_{(0)}^2}{2}+\frac{k_{2t}\varphi_{(\theta_0)}^2}{2}-M_{2z}\varphi(\theta_0)+M_{1z}\varphi(0)-Q_{2y}v(\theta_0)+Q_{1y}v(0)+M_{2x}\frac{\mathrm{d}v(\theta_0)}{R\mathrm{d}\theta}-M_{1x}\frac{\mathrm{d}v(0)}{R\mathrm{d}\theta} \tag{1}$$

where EI_x, GJ, R, and φ are respectively the flexural rigidity, torsional rigidity, center-line radius, and the twist angle. k_l and k_t are liner and torsional elastic coefficients at the support. p_y, t_z, M_{iz}, M_{ix} and Q_{iy} $(i=1,2)$ are the applied distributed transverse load, torque, twisting moment, bending moment and shear force at the boundary, respectively. θ_0 is the sector angle (see Fig. 1). To reach an equilibrium state, the first variation of Eq. (1) must be stationary, that is

$$\delta v: \frac{EI_x}{R^2}\frac{\mathrm{d}^4 v}{\mathrm{d}\theta^4}+\frac{2}{R^2}\frac{\mathrm{d}(EI_x)}{\mathrm{d}\theta}\frac{\mathrm{d}^3 v}{\mathrm{d}\theta^3}+\left[\frac{1}{R^2}\frac{\mathrm{d}^2(EI_x)}{\mathrm{d}\theta^2}-\frac{GJ}{R^2}\right]\frac{\mathrm{d}^2 v}{\mathrm{d}\theta^2}-\frac{1}{R^2}\frac{\mathrm{d}(GJ)}{\mathrm{d}\theta}\frac{\mathrm{d}v}{\mathrm{d}\theta}-\left(\frac{EI_x+GJ}{R}\right)\frac{\mathrm{d}^2\varphi}{\mathrm{d}\theta^2}$$
$$-\frac{1}{R}\frac{\mathrm{d}(2EI_x+GJ)}{\mathrm{d}\theta}\frac{\mathrm{d}\varphi}{\mathrm{d}\theta}-\frac{1}{R}\frac{\mathrm{d}^2(EI_x)}{\mathrm{d}\theta^2}\varphi-p_y R^2=0 \tag{2}$$

$$\delta\varphi: \left(\frac{EI_x+GJ}{R}\right)\frac{\mathrm{d}^2 v}{\mathrm{d}\theta^2}+\frac{1}{R}\frac{\mathrm{d}(GJ)}{\mathrm{d}\theta}\frac{\mathrm{d}v}{d\theta}+GJ\frac{\mathrm{d}^2\varphi}{\mathrm{d}\theta^2}+\frac{\mathrm{d}(GJ)}{\mathrm{d}\theta}\frac{\mathrm{d}\varphi}{\mathrm{d}\theta}-EI_x\varphi-t_z R=0 \tag{3}$$

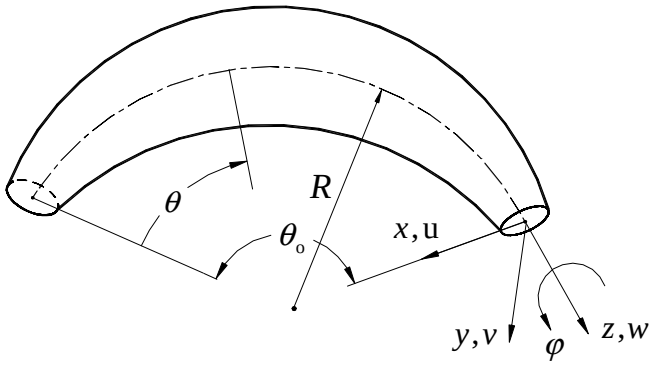

Fig. 1. Geometry of curved arches.

Eqs. (2) and (3) represent the transverse and torsional equilibrium, respectively. The boundary conditions for Eq. (1) are classified as,

(a) $v = 0$ *or shear force is prescribed*

$$Q_y + \frac{1}{R^2}\left[EI_x\left(\frac{1}{R}\frac{\mathrm{d}^3 v}{\mathrm{d}\theta^3} - \frac{\mathrm{d}\varphi}{\mathrm{d}\theta}\right) + \frac{\mathrm{d}(EI_x)}{\mathrm{d}\theta}\left(\frac{1}{R}\frac{\mathrm{d}^2 v}{\mathrm{d}\theta^2} - \varphi\right) - GJ\left(\frac{\mathrm{d}\varphi}{\mathrm{d}\theta} + \frac{1}{R}\frac{\mathrm{d}v}{\mathrm{d}\theta}\right)\right] + nk_1 v = 0 \tag{4}$$

where n is 1 for $\theta = 0$ and -1 for $\theta = \theta_0$.

(b) $\frac{\mathrm{d}v}{\mathrm{d}\theta} = 0$, *or the bending moment is prescribed:*

$$M_x + \frac{EI_x}{R}\left(\frac{1}{R}\frac{\mathrm{d}^2 v}{\mathrm{d}\theta^2} - \varphi\right) = 0 \tag{5}$$

(c) $\varphi = 0$, *or the twisting moment is prescribed:*

$$M_z - \frac{GJ}{R}\left(\frac{\mathrm{d}\varphi}{\mathrm{d}\theta} + \frac{1}{R}\frac{\mathrm{d}v}{\mathrm{d}\theta}\right) + nk_t\varphi = 0 \tag{6}$$

where n is 1 for $\theta = 0$ and -1 for $\theta = \theta_0$. Also, combinations of the above prescribed boundary conditions provide a variety of practical boundary conditions. Some of the boundary conditions (Fig. 2) to be considered here are given in Appendix A.

To simplify the equations, the following definitions are introduced.

$$\begin{aligned} &\Theta = \frac{\theta}{\theta_0}; \quad \mu = \frac{GJ_0}{EI_{ox}} = \frac{GJ}{EI_x} = \frac{1}{1+v}; \quad I_x(\Theta) = I_{ox}H(\Theta); \quad J(\Theta) = J_0 H(\Theta); \\ &K_{\mathrm{L}} = \frac{k_1 R^3}{GJ_0}; \quad K_{\mathrm{T}} = \frac{k_t R}{GJ_0}; \quad P_y = \frac{p_y R^4}{GJ_0}; \quad T_z = \frac{t_z R^2}{GJ_0}; \quad V = \frac{v}{R} \end{aligned} \tag{7}$$

Using these definitions, the equilibrium equations for a variable stiffness circular arch become,

$$\begin{aligned} &HV'''' + 2H'V''' - (\mu\theta_0^2 H - H'')V'' - \mu H'\theta_0^2 V' - (1+\mu)H\theta_0^2\varphi'' - (2+\mu)H'\theta_0^2\varphi' - H''\theta_0^2\varphi + \mu\theta_0^4 KV \\ &\quad - \mu\theta_0^4 P_y = 0 \end{aligned} \tag{8}$$

$$H(1+\mu)V'' + \mu H'V' + \mu H\varphi'' + \mu H'\varphi' - H\theta_0^2\varphi - \mu\theta_0^2 T_z = 0 \tag{9}$$

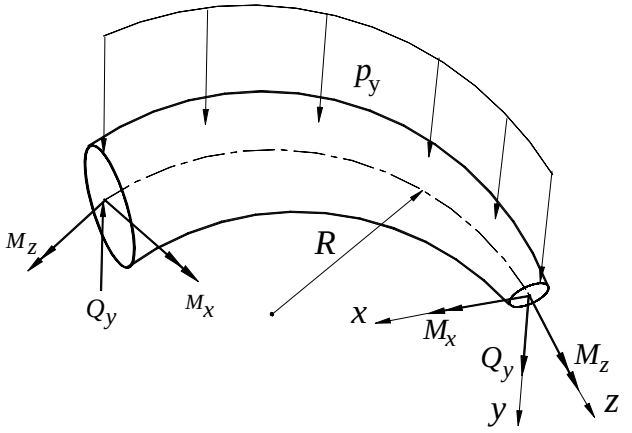

Fig. 2. Loading of a curved arch.

where a single prime denotes a differentiation with respect to Θ. Using Eq. (6), the normalized form of Eq. (4) becomes,

$$H(V''' - \theta_0^2\varphi') + H'(V'' - \theta_0^2\varphi) + n\mu\theta_0^3 K_L V_b + \mu\theta_0^3\left(\frac{Q_y R^2}{GJ_0}\right) - \mu\theta_0^3\left(\frac{M_z R}{GJ_0}\right) - \mu\theta_0^3 n K_T \varphi_b = 0 \tag{10}$$

The normalized forms for the other two types of natural boundary conditions, i.e. Eqs. (5) and (6) would become respectively as,

$$H(V'' - \theta_0^2\varphi) + \mu\theta_0^2\left(\frac{M_x R}{GJ_0}\right) = 0 \tag{11}$$

$$H(\varphi + V') - (n\theta_0 K_T)\varphi - \theta_0\left(\frac{M_z R}{GJ_0}\right) = 0 \tag{12}$$

2.1. DQ analogues of governing and boundary conditions

The degrees of freedom are taken to be V, and φ within the domain and on the boundary, and $K(= V'')$ at the boundary points. Therefore, the vectors of boundary and domain degrees of freedom take the following forms,

$$\{U\}_b^T = [[V_1\ V_2]\ [\varphi_1\ \varphi_2]\ [K_1\ K_2]]; \quad \{U\}_d^T = [[V_2\ \cdots\ V_{N-1}]\ [\varphi_2\ \cdots\ \varphi_{N-1}]] \tag{13}$$

Based on these definitions, the DQ analogues of the governing equations become,
Eq. (8):

$$\begin{aligned} & H_i \sum_{n=1}^{N}\sum_{m=2}^{N-1} B_{im}B_{mn}V_n + 2H_i' \sum_{n=1}^{N}\sum_{m=2}^{N-1} A_{im}B_{mn}V_n - (\mu\theta_0^2 H_i - H_i'')\sum_{m=1}^{N} B_{im}V_m - \mu H_i'\theta_0^2 \sum_{m=1}^{N} A_{im}V_m \\ & - (1+\mu)H_i\theta_0^2 \sum_{m=1}^{N} B_{im}\varphi_m - (2+\mu)H_i'\theta_0^2 \sum_{m=1}^{N} A_{im}\varphi_m - H_i''\theta_0^2\varphi_i + (H_i B_{i1} + 2H_i' A_{i1})K_1 \\ & + (H_i B_{iN} + 2H_i' A_{iN})K_N + \mu\theta_0^4 K_i V_i - \mu\theta_0^4 P_{iy} = 0 \end{aligned} \tag{14}$$

Eq. (9):

$$H_i(1+\mu)\sum_{m=1}^{N} B_{im}V_m + \mu H_i'\sum_{m=1}^{N} A_{im}V_m + \mu H_i\sum_{m=1}^{N} B_{im}\varphi_m + \mu H_i'\sum_{m=1}^{N} A_{im}\varphi_m - H_i\theta_0^2\varphi_i - \mu\theta_0^2 T_z = 0 \tag{15}$$

where A_{ij} and B_{ij} are the weighting coefficients of the first and second-order derivatives, which are obtained using the generalized differential quadrature rule (De Rosa and Franciosi, 1998a; Shu and Richards, 1992). By separating the boundary and the domain degrees of freedom in Eqs. (14) and (15), the DQ analogue equations are obtained in the matrix form as,

$$[S_{db}]\{U\}_b + [S_{dd}]\{U\}_d = \{F\}_d \tag{16}$$

Based on the definitions for the degrees of freedom, one can obtain the elements of coefficient matrices $[S_{db}]$, and $[S_{dd}]$ easily. Similarly, the DQ analogues of the boundary conditions are obtained as:

Displacement is prescribed:

$$V_b = 0 \quad b = 1 \text{ or } N \tag{17}$$

Rotation is prescribed:

$$\varphi_b = 0 \quad b = 1 \text{ or } N \tag{18}$$

Slope is prescribed:

The zero slope boundary conditions are implemented through K at the corresponding boundary points as,

$$K_b - \sum_{k=1}^{N}\sum_{j=ml}^{mu} A_{bj}A_{jk}V_k = 0 \quad \text{for } b = 1 \text{ or } N \tag{19}$$

In the above equation at $\Theta = 0$, $ml = 2$ for zero slope conditions, otherwise $ml = 1$. At edge $\Theta = 1$, $mu = N - 1$ for zero slope condition, otherwise $mu = 1$.

Bending moment is prescribed:

$$H_b(K_b - \theta_0^2\varphi_b) + \mu\theta_0^2\left(\frac{M_{bx}R}{GJ_0}\right) = 0; \quad \text{for } b = 1 \text{ or } N \tag{20}$$

Twisting moment is prescribed:

$$H_b\left(\sum_{j=1}^{N} A_{bj}\varphi_j + \sum_{j=1}^{N} A_{bj}V_j\right) - (n\theta_0 K_{bT})\varphi_b - \theta_0\left(\frac{M_{bz}R}{GJ_0}\right) = 0; \quad \text{for } b = 1 \text{ or } N \tag{21}$$

Shear force is prescribed:

$$\begin{aligned} &H_b\sum_{n=1}^{N}\sum_{m=2}^{N-1} A_{bm}B_{mn}V_n + H_b'(K_b - \theta_0^2\varphi_b) - \theta_0^2 H_b\sum_{m=1}^{N} A_{bm}\varphi_m + H_bA_{b1}K_1 + H_bA_{bN}K_N + n\mu\theta_0^3 K_{bL}V_b \\ &+ \mu\theta_0^3\left(\frac{Q_{by}R^2}{GJ_0}\right) - \mu\theta_0^3\left(\frac{M_{bz}R}{GJ_0}\right) - \mu\theta_0^3 K_{bT}n\varphi_b = 0 \quad \text{for } b = 1 \text{ or } N \end{aligned} \tag{22}$$

The assembled form of the boundary conditions become

$$[S_{bb}]\{U\}_b + [S_{bd}]\{U\}_d = \{F\}_b \tag{23}$$

After eliminating the boundary degrees of freedom, Eq. (23) becomes,

$$[S]\{U\}_d = \{F\} \tag{24}$$

where

$$[S] = [S_{dd}] - [S_{db}][S_{bb}]^{-1}[S_{bd}]; \quad \{F\} = \{F\}_d - [S_{db}][S_{bb}]^{-1}\{F\}_b$$

After evaluating the values for the domain degrees of freedom, one can subsequently obtain the values for the boundary degrees of freedom. The bending and twisting moments at any section of the arch can be obtained as, respectively,

$$\frac{M_{ix}\theta_0^2}{GJ_0} = \frac{H_i}{\mu}\left(\varphi_i\theta_0^2 - \sum_{j=1}^{N} B_{ij}V_j\right) \quad \text{for } i = 2,\ldots,N-1 \tag{25}$$

$$\frac{M_{iz}R\theta_0}{GJ_0} = H_i\left(\sum_{j=1}^{N} A_{ij}\varphi_j + \sum_{j=1}^{N} A_{ij}V_j\right) \quad \text{for } i = 1,\ldots,N \tag{26}$$

It should be mentioned that the bending moments on the boundaries may be obtained from Eq. (20) more accurately.

2.2. Domain decomposition technique

Civan and Sliepcevich (1985) introduced domain decomposition technique with DQM for the first time. When the coefficients in the governing differential equations change within the domain of interest (see Fig. 3), domain decomposition technique may then become a necessity. For such problems, the vector of boundary degrees of freedom should be modified to include the displacements and their second differentiations at the common sections of each of the two adjacent sub-domains. For example, consider section 'i' of the two sub-domains 'i' and '$i+1$'; the new boundary degrees of freedoms at the common section are $[V_{ic}\ \varphi_{ic}\ K_{iL}\ K_{iR}]$. Subscripts 'c', 'L' and 'R' stand for common node, left and right of a common section 'i'. Therefore, the boundary degrees of freedom become,

$$\{U_b\} = [[V_1\ V_N]\ [\varphi_1\ \varphi_N]\ [K_1\ K_N]\ [v_{1c}\ \varphi_{1c}\ K_{1L}\ K_{1R}]\ \ldots\ [v_{N_cc}\ \varphi_{N_cc}\ K_{N_cL}\ K_{N_cR}]]^{T} \tag{27}$$

where N_c is the number of common sections of (N_c+1) sub-domains.

The governing equations of each sub-domain are similar to those of a single domain obtained in Section 2.1. In addition to the external boundary conditions, the geometrical and physical compatibilities should be satisfied at the common sections of the two adjacent sub-domains. The geometrical compatibility conditions include the continuity of tangential and radial displacements, and the slopes. The continuity of the displacement components is automatically satisfied, since they are chosen as the degrees of freedom. The continuity of slopes would be enforced through the following differential quadrature rule,

$$\left(\frac{1}{\theta_i}\right)\sum_{m=1}^{N_i} A_{b_i m}^{(i)} V_m^{(i)} - \left(\frac{1}{\theta_{i+1}}\right)\sum_{m=1}^{N_{i+1}} A_{b_{i+1} m}^{(i+1)} V_m^{(i+1)} = 0 \tag{28}$$

In the above equations 'N_i' represents the number of grid points in sub-domain 'i'. $b_i = N_i$ for ith sub-domain and $b_{i+1} = 1$ for $(i+1)$th sub-domain. Due to the fact that the number of grid points in each sub-domain may be unequal, their weighting coefficients could be different.

The DQ analogues for the equilibrium continuity of torsion, bending moments and shear forces become, respectively,

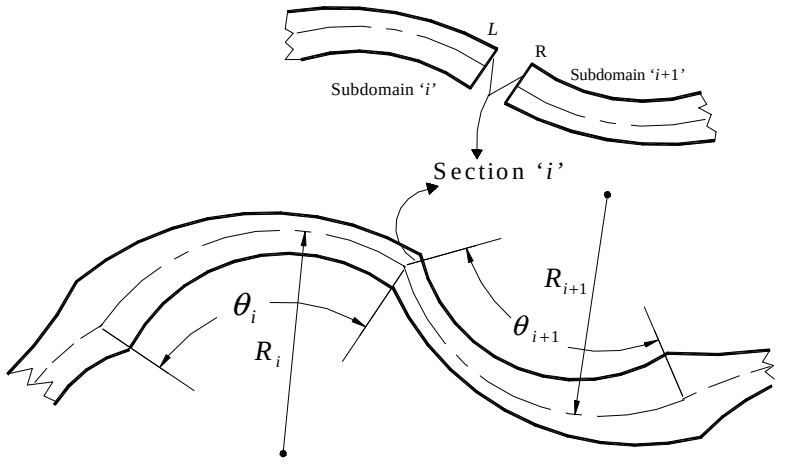

Fig. 3. An arbitrary arch composed of different circular segments.

$$\frac{G^{(i)}J_{b_i}}{R_i}\left[\frac{1}{\theta_i}\sum_{m=1}^{N_i}A_{b_im}^{(i)}(V_m^{(i)}+\varphi_m^{(i)})\right]-\frac{G^{(i+1)}J_{b_{i+1}}}{R_{i+1}}\left[\frac{1}{\theta_{i+1}}\sum_{m=1}^{N_{i+1}}A_{b_{i+1}m}^{(i+1)}(V_m^{(i+1)}+\varphi_m^{(i+1)})\right]=T_i \tag{29}$$

$$\frac{E^{(i)}I_{b_i}}{R_i}\left[-\frac{1}{\theta_i^2}K_{b_i}^{(i)}+\varphi_{b_i}^{(i)}\right]-\frac{E^{(i+1)}I_{b_{i+1}}}{R_{i+1}}\left[-\frac{1}{\theta_{i+1}^2}K_{b_{i+1}}^{(i+1)}+\varphi_{b_{i+1}}^{(i+1)}\right]=M_i \tag{30}$$

$$\begin{aligned}&\frac{E^{(i)}}{R_i^2\theta_i^3}\left[I_{b_i}\sum_{n=1}^{N_i}\sum_{m=2}^{N_i-1}A_{b_im}^{(i)}B_{mn}^{(i)}V_n^{(i)}+I_{b_i}A_{b_i1}^{(i)}K_1^{(i)}+I_{b_i}A_{b_iN_i}^{(i)}K_{N_i}^{(i)}+I'_{b_i}K_{b_i}^{(i)}-I'_{b_i}\theta_i^2\varphi_{b_i}^{(i)}-I_{b_i}\theta_i^2\sum_{m=1}^{N_i}A_{b_im}^{(i)}\varphi_m^{(i)}\right]\\&-\frac{E^{(i+1)}}{R_{i+1}^2\theta_{i+1}^3}\left[I_{b_{i+1}}\sum_{n=1}^{N_{i+1}}\sum_{m=2}^{N_{i+1}-1}A_{b_{i+1}m}^{(i+1)}B_{mn}^{(i+1)}V_n^{(i+1)}+I_{b_{i+1}}A_{b_{i+1}1}^{(i+1)}K_1^{(i+1)}+I_{b_{i+1}}A_{b_{i+1}N_{i+1}}^{(i+1)}K_{N_{i+1}}^{(i+1)}+I'_{b_{i+1}}K_{b_{i+1}}^{(i+1)}\right.\\&\left.-I'_{b_{i+1}}\theta_{i+1}^2\varphi_{b_{i+1}}^{(i+1)}-I_{b_{i+1}}\theta_{i+1}^2\sum_{m=1}^{N_{i+1}}A_{b_{i+1}m}^{(i+1)}\varphi_m^{(i+1)}\right]-\frac{G^{(i)}J_{b_i}}{R_i^2}\left[\frac{1}{\theta_i}\sum_{m=1}^{N_i}A_{b_im}^{(i)}(V_m^{(i)}+\varphi_m^{(i)})\right]\\&+\frac{G^{(i+1)}J_{b_{i+1}}}{R_{i+1}^2}\left[\frac{1}{\theta_{i+1}}\sum_{m=1}^{N_{i+1}}A_{b_{i+1}m}^{(i+1)}(V_m^{(i+1)}+\varphi_m^{(i+1)})\right]=-Q_i\end{aligned} \tag{31}$$

where T_i, M_i and Q_i are the concentrated external twisting moment, bending moment, and shear force at the common section 'i'. The assembled forms of the governing and boundary conditions have similar forms as those of Eqs. (16) and (23).

3. Numerical results

In all the examples non-dimensional transverse displacement (V^*), twist angle (φ^*), bending moment (M_x^*), and twisting moment (M_z^*) are presented according to the following definitions:

Under distributed load (p_y):

$$V^* = V\left(\frac{GJ_0}{p_yR^3}\right) = v\left(\frac{GJ_0}{p_yR^4}\right), \quad \varphi^* = \varphi\left(\frac{GJ_0}{p_yR^3}\right), \quad M_x^* = \frac{M_x}{p_yR^2}, \quad M_z^* = \frac{M_z}{p_yR^2}$$

Under concentrated shear force (Q_y):

$$V^* = V\left(\frac{GJ_0}{Q_yR^2}\right) = v\left(\frac{GJ_0}{Q_yR^3}\right), \quad \varphi^* = \varphi\left(\frac{GJ_0}{Q_yR^2}\right), \quad M_x^* = \frac{M_x}{Q_yR}, \quad M_z^* = \frac{M_z}{Q_yR}$$

In the presence of concentrated twisting moment ($M_z = T$) at boundary:

$$V^* = V\left(\frac{GJ_0}{TR}\right) = v\left(\frac{GJ_0}{TR^2}\right), \quad \varphi^* = \varphi\left(\frac{GJ_0}{TR}\right), \quad M_x^* = \frac{M_x}{T}, \quad M_z^* = \frac{M_z}{T}$$

For arches with discontinuity in stiffness properties (see Fig. 6) instead of J_0, J_1 is used. The Poisson's ratio, υ, is chosen to be 0.3. In all tables, the arc angle (θ_0) of the entire arch or the sub-domain arc angle (θ_{0i}) are usually given. Without loss of generality, the cross-sections are assumed to be circular, except for the ring on elastic foundation. A linear variation in radius size is chosen for the cases of continuously varying cross-sections and thus the following functions for torsional and bending stiffness may be assumed.

$$J = \frac{\pi}{2}r_0^4(1+\alpha\Theta)^4 = J_0(1+\alpha\Theta)^4 = J_0H; \quad I = \frac{\pi}{4}r_0^4(1+\Theta)^4 = I_0(1+\alpha\Theta)^4 = I_0H;$$

r_0 is the section radius of arch at $\theta = 0$.

3.1. Arches with classical boundary conditions

In Table 1, the DQM solution convergency for uniform and continuously varying cross-section cantilever arches subjected to a torque ($M_z = T$) and shear force ($Q_y = -T/R$) at their free ends is examined. As shown the present DQM solutions are matching with the exact solutions up to five significant digits with only 11 grid points ($N = 11$) for the arch with uniform cross-section.

A circular arch problem solved using DQM by Kang et al. (1996) is to be considered here as a benchmark example. They analyzed this arch problem having a constant circular cross-section with both ends simply-supported and/or clamped subjected to end torques. δ-technique have been used to implement the boundary conditions for transverse displacements. Thirteen grid points were employed. They showed that the solution accuracy decreases if δ becomes too small or too large due to numerical instability. They

Table 1
Convergence of results for cantilever circular arc shaft subjected to torque and shear force at free end ($\theta_0 = 180°$; $Q_y = -T/R$)

α	θ		Number of grid points (N)				Exact[a]
			7	9	11	13	
0.0	90°	V^*	−2.3346	−2.3401	−2.3400	−2.3400	−2.3400
		φ^*	−1.2339	−1.2307	−1.2308	−1.2308	−1.2308
		M_z^*	−1.0003	−1.0000	−1.0000	−1.0000	−1.0000
		M_x^*	1.9970	2.0001	2.0000	2.0000	2.0000
−0.4	90°	V^*	−3.1291	−3.1420	−3.1419	−3.1419	–
		φ^*	−2.1799	−2.1361	−2.1350	−2.1350	–
		M_z^*	−1.0152	−1.0007	−1.0000	−1.0000	−1.0000
		M_x^*	2.0009	1.9998	2.0000	2.0000	2.0000

[a] Exact solutions according to Appendix B for the case of $\alpha = 0.0$.

Table 2
Convergence of results for circular arc shaft with both end flexurally simply supported subjected to end torque ($\theta_0 = 90°$)

A	θ		Number of grid points (N)				Exact (Kang et al., 1996)
			7	9	11	13	
0.0	45°	V^*	0.32532	0.32532	0.32532	0.32532	0.32532
		φ^*	−1.11072	−1.11072	−1.11072	−1.11072	−1.11072
0.4	45°	V^*	1.25469	1.25432	1.25430	1.25430	–
		φ^*	−0.40604	−0.40592	−0.40591	−0.40591	–

found the optimal values for δ by a trial and error procedure. Due to anti-symmetric nature of loading and the symmetry of the geometry and boundary conditions, half of the arch is considered here with the following conditions at the middle of arch,

$$v = 0; \quad \varphi = 0; \quad \frac{d^2 v}{d\theta^2} = 0 \quad \text{at } \theta = \theta_0$$

Again the solution convergence behavior for the uniform as well as continuously varying cross-section arch with both ends simply supported and subjected to end torques are shown in Table 2. It is obvious that for prismatic cross-sections (the situation considered by Kang et al., 1996) only seven grid points ($N = 7$) are sufficient here to obtain solutions with five significant digits accuracy. For the same example, but with a variable cross-section and with a taper parameter of $\alpha = 0.4$, 11 grid points were needed to obtain a converged solution with comparable significant digits. It was realized that the twisting and bending moments have similar convergence pattern as those for the twisting angle and displacement.

The results for a uniform cross-section arch with both ends clamped are presented in Table 3. Also, converged solutions for a simply supported arch with continuously varying cross-section for different values of taper parameter are presented in Table 4.

The solutions for a continuously varying cross-section cantilever shaft subjected to a concentrated shear force and twisting moments at its free-end can be found in Table 5. As no exact solutions can be found for tapered arches, to check the validity of the numerical solutions, bending and twisting moments were evaluated at different sections of the shaft using Eqs. (22) and (23). The resulted DQM solutions were then compared with those values obtained from the equilibrium equations for bending and twisting moments prove the validity of the DQM solutions for the field variables v and φ.

3.2. Arches with non-classical boundary conditions

As an example of an arch with non-classical boundary conditions, a uniformly loaded prismatic circular arch with one end ($\theta = 0$) elastically restrained against rotation, and the other end ($\theta = \theta_0$)

Table 3
Results for uniform circular arc shaft with both ends flexurally clamped subjected to end torques ($N = 11$, $\theta_0 = 90°$)[a]

	θ					
	0°	18°	36°	54°	72°	90°
V^*	0.0000	−0.009935	−0.02435	−0.02863	−0.01897	0.0000
Φ^*	−0.8511	−0.5623	−0.3359	−0.1767	−0.07281	0.0000
M_z^*	1.0000	0.7776	0.5770	0.4178	0.3156	0.2803
M_x^*	−0.7197	−0.6844	−0.5822	−0.4230	−0.2224	0.0000

[a] Results in this table match with exact solutions (Kang et al., 1996) to the indicated number of digits.

Table 4
Results for non-uniform circular arc shaft with both ends flexurally simply supported and subjected to end torques ($N = 11$, $\theta_0 = 90°$)[a]

	α	Θ					
		0°	18°	36°	54°	72°	90°
V^*	0.0	0.0000	0.2373	0.3283	0.2950	0.1712	0.0000
	0.2	0.0000	0.1459	0.1977	0.1747	0.1003	0.0000
	0.4	0.0000	0.09689	0.1287	0.1121	0.0638	0.0000
φ^*	0.0	−1.5708	−1.4939	−1.2708	−0.9233	−0.4854	0.0000
	0.2	−1.1030	−0.9583	−0.7609	−0.5231	−0.2625	0.0000
	0.4	−0.83196	−0.6590	−0.4903	−0.3217	−0.1559	0.0000

[a] M_z^* and M_x^* match with exact solutions (Kang et al., 1996) up to five significant digits at any α. V^* and φ^* match with exact solutions (Kang et al., 1996) up to the indicated number of digits at $\alpha = 0$.

Table 5
Results for non-uniform cantilever circular arc shaft subjected to torque and shear force at free end ($N = 11$, $\theta_0 = 180°$, $Q_y = -T/R$)[a]

	α	θ						
		0°	36°	72°	90°	108°	154°	180°
V^*	0.0	0.0000	−0.1181	−1.3012	−2.3400	−3.6471	−6.5628	−8.6998
	−0.2	0.0000	−0.1913	−1.4529	−2.6861	−4.3011	−8.1328	−11.168
	−0.4	0.0000	−0.2026	−1.6414	−3.1419	−5.2148	−10.594	−15.377
Φ^*	0.0	0.0000	−1.6228	−1.8576	−1.2308	−1.3998	2.8739	5.5582
	−0.2	0.0000	−1.7636	−2.2284	−1.5942	−0.3217	3.7078	7.9646
	−0.4	0.0000	−1.9256	−2.7294	−2.1350	−0.6387	5.1972	13.344
M_z^*	Any α	−3.0000	−2.6180	−1.6180	−1.0000	−0.3820	0.6180	1.0000
M_x^*	Any α	0.0000	1.1756	1.9021	2.0000	1.9021	1.1756	0.0000

[a] See footnote of Table 4.

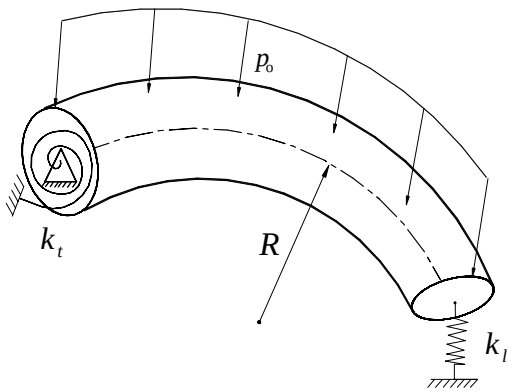

Fig. 4. Uniformly loaded arch with elastically restrained and against rotation and transverse displacement.

elastically restrained against transverse displacement (see Fig. 4) is considered. The exact solutions for this problem were derived and are presented in Appendix B. The DQM solutions are shown in Table 6. Different values for the torsional and linear elastic coefficients are selected and without loss of gene-

Table 6
Results for uniform circular arc shaft with elastically restrained against rotation-elastically restrained against transverse displacement under uniform load ($N = 12$, $\theta_0 = 180°$)[a]

	$K_L = K_T$	θ						
		0°	32.73°	65.46°	98.18°	130.91°	163.64°	180°
V^*	10^{-2}	0.00000	10.258	37.627	73.118	105.19	123.51	125.47
	1.0	0.00000	0.3582	1.1970	1.9846	2.2137	1.6765	1.1681
	10^2	0.00000	0.2380	0.7771	1.2086	1.1551	0.5021	0.01095
	10^6	0.00000	0.2366	0.7724	1.2002	1.1442	0.4907	0.00000
C-S supports		0.00000	0.2366	0.7724	1.2002	1.1442	0.4907	0.00000
φ^*	10^{-2}	63.241	53.034	25.364	−10.523	−42.784	−61.300	−63.266
	1.0	0.8054	0.6210	−0.4368	−1.5641	−2.0471	−1.6017	−1.0976
	10^2	0.000952	0.02699	−0.6621	−1.3856	−1.5612	−0.9930	−0.5057
	10^6	0.000000	0.02038	−0.6641	−1.3831	−1.5556	−0.9867	−0.5000
C-S supports		0.000000	0.02038	−0.6641	−1.3831	−1.5556	−0.9867	−0.5000
M_z^*	10^{-2}	0.6321	−0.2805	−0.6864	−0.6380	−0.3320	−0.4696	0.0000
	1.0	0.8054	−0.1210	−0.5638	−0.5637	−0.3021	−0.04345	0.0000
	10^2	0.9522	0.01414	−0.4599	−0.5007	−0.2768	−0.04048	0.0000
	10^6	0.9549	0.01666	−0.4579	−0.4996	−0.2763	−0.04042	0.0000
C-S supports		0.9549	0.01666	−0.4579	−0.4996	−0.2763	−0.04042	0.0000
M_x^*	10^{-2}	−2.0000	−1.1629	−0.2741	0.3843	0.6031	0.3130	0.0000
	1.0	−2.0000	−1.2097	−0.3529	0.2985	0.5376	0.2886	0.0000
	10^2	−2.0000	−1.2494	−0.4196	0.2259	0.4822	0.2679	0.0000
	10^6	−2.0000	−1.2502	−0.4209	0.2245	0.4811	0.2675	0.0000
C-S supports		−2.0000	−1.2502	−0.4209	0.2245	0.4811	0.2675	0.0000

[a] Results in this table match with exact solutions (Appendix B) up to the indicated number of digits.

rality, their non-dimensional values are taken to be equal, i.e. $K_T = K_L$. One should note that the rigid body motion (torsional rotation) causes the displacements and also the rotations to increase as the values of the support elastic coefficients at the ends are reduced. Also, when the elastic coefficients become very large, i.e. K_T, $K_L \geqslant 10^2$, the results would converge to those results of a clamped-simply (C-S) supported arch. The results were obtained with $N = 12$, although satisfactory accurate results may be obtained with $N = 9$, especially for the cases that K_T, $K_L \geqslant 1$. Similar to previous examples, excellent agreements with corresponding exact solutions at different values for elastic coefficients are achieved.

3.3. Examples with domain decomposition technique

In this section example problems that need domain decomposition technique are to be considered. The exact solutions for these problems are either derived by the authors as presented in Appendix B or have been taken from the work by Volterra (1951).

3.3.1. Ring on elastic foundations with point loads

A ring on elastic foundation with a series of point loads is considered (see Fig. 5). Volterra (1951) presented an analytical solution for this uniform section circular ring on elastic foundation. Due to point loads, global basis or test functions cannot be used to evaluate the weighting coefficients and therefore the adoption of the domain decomposition technique becomes a necessity. Due to symmetry of the geometry and loading condition, with n concentrated forces, only $(1/n)$ of the ring is considered. The geometry of the

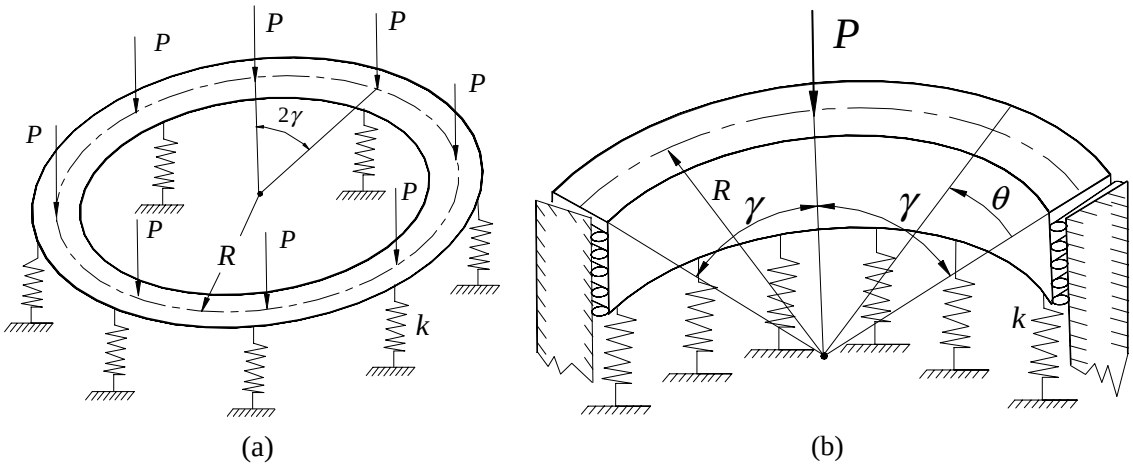

Fig. 5. (a) A Ring on elastic foundation subjected to point loads (b) Geometry of the modeling.

Table 7
Convergence of the results for uniform circular ring on elastic foundation subjected to point loads ($2\gamma = 180°$, $\mu = 1$)[a]

	N	θ ($K = 1$)				θ ($K = 100$)			
		0.0°	30°	60°	90°	0.0°	30°	60°	90°
$10^2 \times V^*$	7	24.323	27.845	35.511	39.980	−0.08976	−0.03368	0.4479	1.1762
	10	24.325	27.844	35.508	39.978	−0.1091	−0.04038	0.4622	1.1964
	13	24.325	27.844	35.508	39.978	−0.1092	−0.04045	0.4621	1.1960
	16	24.325	27.844	35.508	39.978	−0.1092	−0.04045	0.4621	1.1960
$10^2 \times \varphi^*$	7	11.941	6.4028	−5.8330	−13.163	0.5823	0.5655	−0.1629	−1.4524
	10	11.939	6.4069	−5.8218	−13.150	0.6381	0.5885	−0.1842	−1.4916
	13	11.939	6.4069	−5.8218	−13.150	0.6392	0.5891	−0.1836	−1.4904
	16	11.939	6.4069	−5.8218	−13.150	0.6392	0.5891	−0.1836	−1.4904
$10^2 \times M_z^*$	7	0.0000	−7.2254	−8.8516	0.0000	0.0000	−0.00816	−1.0615	0.0000
	10	0.0000	−7.2170	−8.8431	0.0000	0.0000	−0.05358	−1.1051	0.0000
	13	0.0000	−7.2170	−8.8431	0.0000	0.0000	−0.05421	−1.1048	0.0000
	16	0.0000	−7.2170	−8.8431	0.0000	0.0000	−0.05421	−1.1048	0.0000
$10^2 \times M_x^*$	7	−15.612	−10.173	5.5530	29.234	0.5117	−1.0288	−2.2564	10.191
	10	−15.600	−10.168	5.5486	29.221	0.3868	−1.0199	−2.2400	10.499
	13	−15.600	−10.168	5.5486	29.221	0.3856	−1.0186	−2.2382	10.498
	16	−15.600	−10.168	5.5486	29.221	0.3856	−1.0186	−2.2382	10.498

[a] Results in this table match with exact solutions (Volterra, 1951) up to the indicated number of digits.

model is shown in Fig. 5(b) and the boundary conditions at its ends are stated in Appendix A. Two subdomains are sufficient for the analysis of this problem. Three different loading conditions are considered and in each case different values for the elastic foundation are examined. In Table 7, the solution convergence is shown for the ring under only two point loads, the least number of point loads for a symmetric loading. In Table 8, the results for the cases that the numbers of point loads are relatively large are exhibited. Also, the results for an intermediate number of point loads are presented in Table 9. By comparing the results for these cases one can conclude that in all cases using $N \leqslant 13$ can yield a converged solution for

Table 8
Convergence of the results for uniform circular ring on elastic foundation subjected to point loads ($2\gamma = 30°$, $\mu = 1$)[a]

	N	θ ($K = 1$)				θ ($K = 100$)			
		0.0°	5°	10°	15°	0.0°	5°	10°	15°
$10^2 \times V^*$	7	190.97	190.98	190.99	191.01	1.8921	1.9001	1.9184	1.9301
	13	190.97	190.98	190.99	191.01	1.8921	1.9001	1.9184	1.9301
$10^3 \times \varphi^*$	7	0.3540	0.1946	−0.1706	−0.4040	0.3524	0.1939	−0.1694	−0.4020
	13	0.3540	0.1946	−0.1706	−0.4040	0.3524	0.1939	−0.1694	−0.4020
$10^2 \times M_z^*$	7	0.0000	−0.1705	−0.2129	0.0000	0.0000	−0.1696	−0.2120	0.0000
	13	0.0000	−0.1705	−0.2129	0.0000	0.0000	−0.1696	−0.2120	0.0000
$10^2 \times M_x^*$	7	−2.1991	−1.4640	0.7356	4.3833	−2.1863	−1.4575	0.7293	4.7301
	13	−2.1991	−1.4640	0.7356	4.3833	−2.1863	−1.4575	0.7293	4.7301

[a] Results in this table match with exact solutions (Volterra, 1951) up to the indicated number of digits.

Table 9
Convergence of the results for uniform circular ring on elastic foundation subjected to point loads ($2\gamma = 90°$, $\mu = 1$)[a]

	N	θ ($K = 1$)				θ ($K = 100$)			
		0.0°	15°	30°	45°	0.0°	15°	30°	45°
$10^2 \times V^*$	7	63.091	63.352	63.938	64.303	0.2552	0.4215	0.8185	1.0874
	10	63.091	63.352	63.938	64.303	0.2552	0.4217	0.8185	1.0868
	13	63.091	63.352	63.938	64.303	0.2552	0.4217	0.8185	1.0868
$10^2 \times \varphi^*$	7	1.0717	0.5848	−0.5186	−1.2108	0.7214	0.4109	−0.3356	−0.8478
	10	1.0719	0.5851	−0.5183	−1.2106	0.7158	0.4055	−0.3403	−0.8512
	13	1.0719	0.5851	−0.5183	−1.2106	0.7158	0.4055	−0.3403	−0.8512
$10^2 \times M_z^*$	7	0.0000	−1.6260	−2.0133	0.0000	0.0000	−1.0524	−1.4294	0.0000
	10	0.0000	−1.6260	−2.0133	0.0000	0.0000	−1.0506	−1.4271	0.0000
	13	0.0000	−1.6260	−2.0133	0.0000	0.0000	−1.0506	−1.4271	0.0000
$10^2 \times M_x^*$	7	−7.0093	−4.6191	2.4051	13.622	−4.3683	−3.2557	−1.0892	10.876
	10	−7.0093	−4.6191	2.4051	13.622	−4.3727	−3.2567	−1.0932	10.883
	13	−7.0093	−4.6191	2.4051	13.622	−4.3727	−3.2567	−1.0932	10.883

[a] Results in this table match with exact solutions (Volterra, 1951) up to the indicated number of digits.

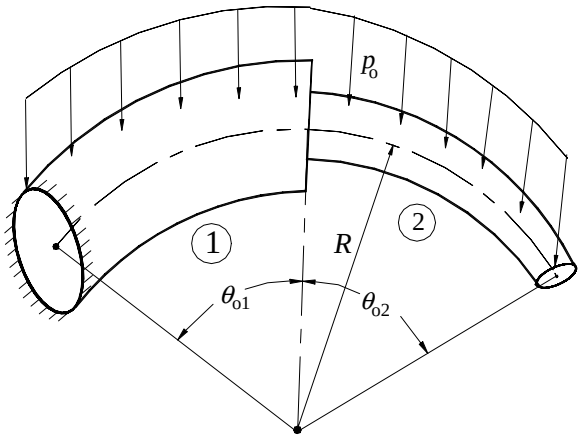

Fig. 6. A cantilever arch with discontinuity in stiffness.

Table 10
Results for stepped arc shaft with clamped-free ends subjected to uniform loads ($N = 9$, $\theta_{01} = \theta_{02} = 90°$)[a]

e		θ						
		0°	22.5°	45°	90°	135°	157.5°	180°
2	V^*	0.0000	0.0073	0.3271	1.3591	2.6952	3.2226	3.5104
	Φ^*	0.0000	0.4673	0.6060	−0.0086	−1.1265	−1.6393	−1.9261
	M_z^*	3.1416	2.3662	1.6491	0.5708	0.0078	0.00100	0.00000
	M_x^*	−2.0000	−1.9239	−1.7071	−1.0000	−0.2929	−0.00761	0.00000
4	V^*	0.0000	0.0365	0.1636	0.6796	1.4469	1.8010	2.0290
	Φ^*	0.0000	0.2337	0.3030	−0.0043	−0.5534	−0.8928	−1.1200
	M_z^*	3.1416	2.3662	1.6491	0.5708	0.0078	0.00100	0.00000
	M_x^*	−2.0000	−1.9239	−1.7071	−1.0000	−0.2929	−0.00761	0.00000

[a] Results in this table match with exact solutions (Appendix B) up to the indicated number of digits.

the problem. As expected, when the number of point loads is increased (see Table 8), the transverse displacement at each section converges to a unique value and the rotation approaches zero. This is because the loading conditions approaches to a uniform loading condition for which the transverse displacements at all section should become equal and the rotation should tend to zero. Using similar procedure, the domain decomposition technique can be implemented for non-uniform rings under non-symmetric loading.

3.3.2. An arch with discontinuous geometrical and material properties

A cantilever arch with discontinuity in its stiffness subjected to a uniform loading is considered (see Fig. 6). It is assumed both sub-domains have equal Poisson's ratio ($=0.3$) but their Young's moduli would be different. Exact solutions for this problem are given in Appendix B. In Table 10, DQM solutions are presented. Using nine grid points at each sub-domain yields solutions accurate to five significant digits. Different stiffness ratios i.e. $e = \frac{G_1 J_1}{G_2 J_2} = \frac{E_1 I_{1x}}{E_2 I_{2x}}$ were examined.

4. Closure

A DQ methodology was employed to study the out-of-plane static analysis of circular arches with uniform, continuously varying, and stepped cross-sections and under different loading and boundary conditions. The domain decomposition technique in conjunction with the proposed DQ methodology is utilized for the analysis of arches having discontinuity in loading, material and geometry. For uniform and stepped section arches, the solutions were compared with those of exact solutions where the accuracy and the convergence of the methodology were verified under different classical and non-classical boundary conditions. For non-uniform section arches, convergent solutions were obtained and the validity of the results was discussed. Using the present DQ methodology with small number of grid points, accurate and converged solutions for arch problems can be obtained.

Appendix A. The boundary conditions

The boundary conditions considered are of the following types:

(a) Flexurally simply support:

$$v = 0; \quad M_x = \frac{EI_x}{R}\left(-\frac{1}{R}\frac{\mathrm{d}^2 v}{\mathrm{d}\theta^2} + \varphi\right) = 0; \quad M_z = \frac{GJ}{R}\left(\frac{\mathrm{d}\varphi}{\mathrm{d}\theta} + \frac{1}{R}\frac{\mathrm{d}v}{\mathrm{d}\theta}\right) = 0 \tag{A.1}$$

(b) Flexurally clamped:

$$v = 0; \quad \frac{\mathrm{d}v}{\mathrm{d}\theta} = 0; \quad M_z = \frac{GJ}{R}\left(\frac{\mathrm{d}\varphi}{\mathrm{d}\theta} + \frac{1}{R}\frac{\mathrm{d}v}{\mathrm{d}\theta}\right) = 0 \tag{A.2}$$

(c) Clamped:

$$v = 0; \quad \varphi = 0; \quad \frac{\mathrm{d}v}{\mathrm{d}\theta} = 0; \tag{A.3}$$

(d) Elastically restrained against torsional rotation:

$$v = 0; \quad M_x = \frac{EI_x}{R}\left(-\frac{1}{R}\frac{\mathrm{d}^2 v}{\mathrm{d}\theta^2} + \varphi\right) = 0; \quad -\frac{GJ}{R}\left(\frac{\mathrm{d}\varphi}{\mathrm{d}\theta} + \frac{1}{R}\frac{\mathrm{d}v}{\mathrm{d}\theta}\right) + nk_t\varphi = 0 \tag{A.4}$$

(e) Elastically restrained against transverse displacement or free end:

$$\frac{1}{R^2}\left[EI_x\left(\frac{1}{R}\frac{\mathrm{d}^3 v}{\mathrm{d}\theta^3} - \frac{\mathrm{d}\varphi}{\mathrm{d}\theta}\right) + \frac{\mathrm{d}(EI_x)}{\mathrm{d}\theta}\left(\frac{1}{R}\frac{\mathrm{d}^2 v}{\mathrm{d}\theta^2} - \varphi\right) - GJ\left(\frac{\mathrm{d}\varphi}{\mathrm{d}\theta} + \frac{1}{R}\frac{\mathrm{d}v}{\mathrm{d}\theta}\right)\right] + nk_l v = 0$$

$$M_x = \frac{EI_x}{R}\left(-\frac{1}{R}\frac{\mathrm{d}^2 v}{\mathrm{d}\theta^2} + \varphi\right) = 0; \quad M_z = \frac{GJ}{R}\left(\frac{\mathrm{d}\varphi}{\mathrm{d}\theta} + \frac{1}{R}\frac{\mathrm{d}v}{\mathrm{d}\theta}\right) = 0 \tag{A.5}$$

(f) Boundary conditions for each end of the model presented for ring on elastic foundation:

$$\frac{\mathrm{d}v}{\mathrm{d}\theta} = 0; \quad M_z = \frac{GJ}{R}\left(\frac{\mathrm{d}\varphi}{\mathrm{d}\theta} + \frac{1}{R}\frac{\mathrm{d}v}{\mathrm{d}\theta}\right) = 0;$$

$$Q_y = \frac{1}{R^2}\left[EI_x\left(\frac{1}{R}\frac{\mathrm{d}^3 v}{\mathrm{d}\theta^3} - \frac{\mathrm{d}\varphi}{\mathrm{d}\theta}\right) + \frac{\mathrm{d}(EI_x)}{\mathrm{d}\theta}\left(\frac{1}{R}\frac{\mathrm{d}^2 v}{\mathrm{d}\theta^2} - \varphi\right) - GJ\left(\frac{\mathrm{d}\varphi}{\mathrm{d}\theta} + \frac{1}{R}\frac{\mathrm{d}v}{\mathrm{d}\theta}\right)\right] = 0 \tag{A.6}$$

Appendix B. The exact solutions

B.1. Exact solutions for prismatic arches

The works by Volterra (1951) and Kang et al. (1996) can be extended to obtain the exact solutions for differential governing equations of prismatic arches under uniform loading and general boundary conditions. The general solutions under such situations take the following form,

$$V^*(\Theta) = -C_1\cos\Theta - C_2\sin\Theta - \Theta(C_3\sin\Theta + C_4\cos\Theta) + \frac{2(-C_3\cos\Theta + C_4\sin\Theta)}{(1+\mu)} + C_5\Theta + C_6 - \mathrm{sgn}(p_y)(\Theta^2/2) \tag{B.1}$$

$$\varphi^*(\Theta) = C_1\cos\Theta + C_2\sin\Theta + \Theta(C_3\sin\Theta + C_4\cos\Theta) - \mathrm{sgn}(p_y)(1+\mu) \tag{B.2}$$

where

$$\Theta = \theta/\theta_0 \quad \text{and} \quad \mathrm{sgn}(p_y) = \begin{cases} 1 & \text{if } p_y \text{ is positive} \\ -1 & \text{if } p_y \text{ is negative} \end{cases}$$

In the above equations, $\{C\} = [C_1, C_2, C_3, C_4, C_5, C_6]^{\mathrm{T}}$ are obtained after the implementation of the boundary conditions. In the absence of uniform loading, the last terms in Eqs. (B.1) and (B.2) should be removed. The bending and twisting moments are evaluated from Eqs. (B.1) and (B.2) as,

$$M_x^*(\Theta) = \frac{2}{(1+\mu)}(C_3\cos\Theta - C_4\sin\Theta) - \mathrm{sgn}(p_y) \tag{B.3}$$

$$M_z^*(\Theta) = \frac{2}{(1+\mu)}(C_3\sin\Theta + C_4\cos\Theta) + C_5 - \Theta\,\mathrm{sgn}(p_y) \tag{B.4}$$

Also, $\{C\} = [C_1, C_2, C_3, C_4, C_5, C_6]^{\mathrm{T}}$ under different boundary and loading conditions are,

(a) Prismatic cantilever shaft subjected to end twisting moment and shear force:

$$C_1 = -1 + \frac{(1-\mu)}{\cos\theta_0};\quad C_2 = \frac{(1+\mu)\sin\theta_0}{\cos^2\theta_0};\quad C_3 = \frac{1+\mu}{\cos\theta_0};\quad C_4 = -1 \tag{B.5}$$

(b) Elastically restrained prismatic shaft subjected to uniform transverse load:

$$\{C\} = \begin{bmatrix} -K_{\mathrm{T}} & 0 & 0 & 2/(1+\mu) & 1 & 0 \\ -1 & 0 & -2/(1+\mu) & 0 & 0 & 1 \\ 0 & -1 & 0 & (1-\mu)/(1+\mu) & 1 & 0 \\ \mu K_{\mathrm{L}}\cos\theta_0 & \mu K_{\mathrm{L}}\sin\theta_0 & \alpha_1 & \beta_1 & -\mu K_{\mathrm{L}}\theta_0 & -\mu K_{\mathrm{L}} \\ 0 & 0 & \sin\theta_0 & \cos\theta_0 & 0.5(1+\mu) & 0 \\ 0 & 0 & \cos\theta_0 & -\sin\theta_0 & 0 & 0 \end{bmatrix}^{-1} \begin{Bmatrix} -(1+\mu)K_{\mathrm{T}} \\ 0 \\ 0 \\ -\frac{\mu K_{\mathrm{L}}\theta_0^2}{2} \\ \frac{(1+\mu)\theta_0}{2} \\ \frac{(1+\mu)}{2} \end{Bmatrix} \tag{B.6}$$

where

$$\alpha_1 = [(2\mu\sin\theta_0 + 2\mu K_{\mathrm{L}}\cos\theta_0)/(1+\mu)] + \mu K_{\mathrm{L}}\theta_0\sin\theta_0;$$
$$\beta_1 = [(2\mu\cos\theta_0 - 2\mu K_{\mathrm{L}}\sin\theta_0)/(1+\mu)] + \mu K_{\mathrm{L}}\theta_0\cos\theta_0;$$

(c) Clamped-simply (C-S) supported arch under uniform load:

$$\{C\} = \begin{bmatrix} 1 & 0 & 0 & 0 & 0 & 0 \\ -1 & 0 & -2/(1+\mu) & 0 & 0 & 1 \\ 0 & -1 & 0 & (1-\mu)/(1+\mu) & 1 & 0 \\ \mu\cos\theta_0 & \mu\sin\theta_0 & \alpha_2 & \beta_2 & -\mu\theta_0 & -\mu \\ 0 & 0 & \sin\theta_0 & \cos\theta_0 & 0.5(1+\mu) & 0 \\ 0 & 0 & \cos\theta_0 & -\sin\theta_0 & 0 & 0 \end{bmatrix}^{-1} \begin{Bmatrix} -(1+\mu) \\ 0 \\ 0 \\ -\frac{\mu\theta_0^2}{2} \\ \frac{(1+\mu)\theta_0}{2} \\ \frac{(1+\mu)}{2} \end{Bmatrix} \tag{B.7}$$

where

$$\alpha_2 = 2\mu\sin\theta_0/(1+\mu);\quad \beta_2 = [-2\mu\sin\theta_0/(1+\mu)] + \mu\theta_0\cos\theta_0.$$

B.2. Exact solutions for a cantilever shaft with discontinuous stiffness

By using Eqs. (B.1)–(B.4) for each sub-domain and satisfying the boundary as well as the continuity conditions, exact solutions for a cantilever shaft having discontinuous stiffness ($\theta_{01} = \theta_{02}$) subjected to uniform transverse loading (see Fig. 6) are obtained as

(a) In sub-domain 1(see Fig. 6):

$$V^*(\Theta) = -C_1\cos\Theta - C_2\sin\Theta - \Theta(C_3\sin\Theta + C_4\cos\Theta) + \frac{2}{1+\mu}(-C_3\cos\Theta + C_4\sin\Theta) + C_5\Theta + C_6 - (\Theta^2/2e)\mathrm{sgn}(p_y) \tag{B.8}$$

$$\varphi^*(\Theta) = C_1\cos\Theta + C_2\sin\Theta + \Theta(C_3\sin\Theta + C_4\cos\Theta) - \frac{(1+\mu)}{e}\mathrm{sgn}(p_y) \tag{B.9}$$

$$M_x^*(\Theta) = \frac{2e}{(1+\mu)}(-C_3\cos\Theta + C_4\sin\Theta) - \mathrm{sgn}(p_y) \tag{B.10}$$

$$M_z^*(\Theta) = \frac{2e}{(1+\mu)}(C_3\sin\Theta + C_4\cos\Theta) + eC_5 - \Theta\mathrm{sgn}(p_y) \tag{B.11}$$

where

$\Theta = \theta/\theta_{01}$

(b) In sub-domain 2 (see Fig. 6):

$$V^*(\Theta) = -C_7\cos\Theta - C_8\sin\Theta - \Theta(C_9\sin\Theta + C_{10}\cos\Theta) + \frac{2(-C_9\cos\Theta + C_{10}\sin\Theta)}{(1+\mu)} + C_{11}\Theta + C_{12} - 0.5\Theta^2\mathrm{sgn}(p_y) \tag{B.12}$$

$$\varphi^*(\Theta) = C_7\cos\Theta + C_8\sin\Theta + \Theta(C_9\sin\Theta + C_{10}\cos\Theta) - (1+\mu)\mathrm{sgn}(p_y) \tag{B.13}$$

$$M_x^*(\Theta) = \frac{2}{(1+\mu)}(-C_9\cos\Theta + C_{10}\sin\Theta) - \mathrm{sgn}(p_y) \tag{B.14}$$

$$M_z^*(\Theta) = \frac{2}{(1+\mu)}(C_9\sin\Theta + C_{10}\cos\Theta) + C_{11} - \Theta\mathrm{sgn}(p_y) \tag{B.15}$$

where

$\Theta = (\theta - \theta_{01})/\theta_{02}$

θ is measured from the fixed end (see Fig. 6).

Also, $\{C\} = [C_1, C_2, C_3, C_4, C_5, C_6, C_7, C_8, C_9, C_{10}, C_{11}, C_{12}]^{\mathrm{T}}$ are obtained from the solution to the following matrix equation

$$\{C\}=\begin{bmatrix}
-1 & 0 & 0 & 0 & 0 & 0 & 0 & 0 & 0 & 0 & 0 & 0\\
1 & 0 & \frac{2}{(1+\mu)} & 0 & 0 & -1 & 0 & 0 & 0 & 0 & 0 & 0\\
0 & 1 & 0 & -\frac{(\mu-1)}{(1+\mu)} & 1 & 0 & 0 & 0 & 0 & 0 & 0 & 0\\
0 & 0 & 0 & 0 & 0 & 0 & 0 & 0 & -\sin\theta_{01} & -\cos\theta_{01} & 0 & 0\\
0 & 0 & 0 & 0 & 0 & 0 & 0 & 0 & -\sin\theta_{01} & -\cos\theta_{01} & -0.5(1+\mu) & 0\\
0 & 0 & 0 & 0 & 0 & 0 & 0 & 0 & -\cos\theta_{01} & \sin\theta_{01} & 0 & 0\\
0 & -1 & -\theta_{01} & 0 & 0 & 0 & 1 & 0 & 0 & 0 & 0 & 0\\
0 & 1 & \theta_{01} & \frac{-2}{(1+\mu)} & -\theta_{01} & 1 & 1 & 0 & \frac{-2}{(1+\mu)} & 0 & 0 & 1\\
-1 & 0 & \frac{(\mu-1)}{(1+\mu)} & 0 & 0 & 0 & 0 & -1 & 0 & \frac{(1-\mu)}{(1+\mu)} & 1 & 0\\
0 & 0 & -\frac{2e}{(1+\mu)} & 0 & -e & 0 & 0 & 0 & 0 & \frac{2}{(1+\mu)} & 1 & 0\\
0 & 0 & 0 & -\frac{2e\mu}{(1+\mu)} & 0 & 0 & 0 & 0 & \frac{2\mu}{(1+\mu)} & 0 & 0 & 0\\
0 & 0 & -e & 0 & 0 & 0 & 0 & 0 & 0 & 1 & 0 & 0
\end{bmatrix}^{-1}\begin{Bmatrix}
\frac{-(1+\mu)}{e}\\
0\\
0\\
0\\
-\frac{(1+\mu)\theta_{01}}{2}\\
-\frac{(1+\mu)}{2}\\
\left(1-\frac{1}{e}\right)\left(\frac{1+\mu}{2}\right)\\
-\frac{\theta_{01}^2}{8e}\\
-\frac{\theta_{01}}{e}\\
-\theta_{01}\\
0\\
0
\end{Bmatrix} \tag{B.16}$$

References

Bert, C.W., Malik, M., 1996. Differential quadrature method in computational mechanics: a review. Applied Mechanic Review 49, 1–27.

Bert, C.W., Malik, M., 1997. Differential quadrature method: a powerfull new technique for analysis of composite structures. Computers and Structures 39, 179–189.

Chen, W., Striz, A.G., Bert, C.W., 1997. A new approach to the differential quadrature method for fourth-order equations. International Journal for Numerical Methods in Engineering 40, 1941–1956.

Civan, F., Sliepcevich, C.M., 1985. Application of differential quadrature in solution of pool boiling in cavities. Proceeding of Oklahoma Academy of Sciences 65, 73–78.

De Rosa, M.A., Franciosi, C., 1998a. On natural boundary conditions on DQM. Mechanics Research Communication 25, 279–286.

De Rosa, M.A., Franciosi, C., 1998b. Nonclassical boundary conditions and DQM. Journal of Sound and Vibration 212, 743–748.

De Rosa, M.A., Franciosi, C., 2000. Exact and approximate dynamic analysis of circular arches using DQM. International Journal of Solids and Structures 37, 1103–1117.

Kang, K., Bert, C.W., Striz, A.G., 1996. Static analysis of curved shaft subjected to end torques. International Journal of Solids and Structures 11, 1587–1596.

Karami, G., Malekzadeh, P., 2002a. A new differential quadrature methodology for beam analysis and the associated DQEM. Computer Methods in Applied Mechanics and Engineering 191, 3509–3526.

Karami, G., Malekzadeh, P., 2002b. Static and stability analyses of arbitrary straight-sided quadrilateral thin plates by DQM. International Journal of Solids and Structures 39 (19), 4927–4947.

Karami, G., Malekzadeh, P., 2003a. Application of a new differential quadrature methodology for free vibration analysis of plates. International Journal for Numerical Methods in Engineering 54 (3), 847–868.

Karami, G., Malekzadeh, P., 2003b. An efficient differential quadrature methodology for free vibration analysis of arbitrary straight-sided quadrilateral thin plates. Journal of Sound and Vibration 263 (2), 415–442.

Malik, M., Bert, C.W., 1996. Implementing multiple boundary conditions in the DQ solution of higher order PDE's: application to free vibration of plates. International Journal for Numerical Methods in Engineering 39, 1237–1258.

Shu, C., Du, H., 1997a. Implementation of clamped and simply supported boundary conditions in the GDQ free vibration analysis of beams and plates. International Journal of Solids and Structures 34, 819–835.

Shu, C., Du, H., 1997b. A generalized approach for implementing general boundary conditions in the GDQ free vibration analysis of plates. International Journal of Solids Structures 34, 837–846.

Shu, C., Richards, B.E., 1992. Application of generalized differential quadrature to solve two-dimensional incompressible Navier–Stokes equations. International Journal of Numerical Methods in Fluids 15, 791–798.

Tong, X., Mrad, N., Tabrrok, B., 1998. In-plane vibration of circular arches with variable cross-section. Journal of Sound and Vibration 212, 121–140.

Volterra, E., 1951. Bending of a circular beam on elastic foundation. Journal of Applied Mechanics 19, 1–4.

Wang, X., Bert, C.W., 1993. A new approach in applying differential quadrature and free vibrational analysis of beams and plates. Journal of Sound Vibration 162, 566–572.

Wang, X., Gu, H., 1997. Static analysis of frame structures by the differential quadrature element method. International Journal for Numerical Methods in Engineering 40, 759–772.

Wang, X., Wang, Y.L., Chen, R.-B., 1998. Static and free vibration analysis of rectangular plates by the differential quadrature element method. Communications in Numerical Methods in Engineering 14, 1133–1141.

Wu, T.Y., Liu, G.R., 2000. Axisymmetric bending solution of shells of revolution by the generalized differential quadrature rule. International Journal of Pressure Vessel and Piping 77, 149–157.

Wu, T.Y., Liu, G.R., 2001. The generalized differential quadrature rule for fourth-order differential equations. International Journal for Numerical Methods in Engineering 50, 1907–1929.

Yoo, C.H., Fehrenbach, J.P., 1981. Natural frequencies of curved girders. Journal of Engineering Mechanics Division ASCE 107 (EM2), 339–354.